Available online at www.sciencedirect.com

jmr&t Journal of Materials Research and Technology

www.jmrt.com.br

Original Article

The moment of inertia method to calculate equivalent ranges in non-proportional tension–torsion histories

*Marco Antonio Meggiolaro**, *Jaime Tupiassú Pinho de Castro*

Department of Mechanical Engineering, Pontifícia Universidade Católica do Rio de Janeiro, Rio de Janeiro, RJ, Brazil

ARTICLE INFO

Article history:
Received 6 November 2012
Accepted 12 January 2015
Available online 16 March 2015

Keywords:
Multiaxial fatigue
Non-proportional loading
Equivalent stress range

ABSTRACT

A critical issue in multiaxial damage calculation in non-proportional (NP) histories is to find the equivalent stress or strain ranges and mean components associated with each rainflow-counted cycle of the stress (or strain) path. A traditional way to find such ranges is to use enclosing surface methods, which search for convex enclosures, such as balls or prisms, of the entire history path in stress or strain diagrams. These methods only work for relatively simple load histories, since the enclosing surfaces lose information of the original history. This work presents an approach to evaluate equivalent stress and strain ranges in NP histories, called the moment of inertia (MOI) method. It is an integral approach that assumes the path contour in the stress diagram is a homogeneous wire with a unit mass. The center of mass of such wire gives then the mean component of the path, while the moments of inertia of the wire can be used to obtain the equivalent stress or strain ranges. Experimental results obtained from the literature for 13 different multiaxial histories prove the effectiveness of the MOI method to predict fatigue lives.

1. Introduction

Multiaxial fatigue lives can be calculated from equivalent stress (or strain) ranges and their mean components [1]. However, estimating such ranges and mean values for non-proportional (NP) loading cycles is not an easy task. These components are traditionally estimated by convex circular, ellipsoidal, or prismatic enclosures of the entire history path in stress or strain diagrams [2–9]. But enclosing surface methods are not suited for complex NP histories, since they do not account for path shape dependence of fatigue damage.

Consider a periodic load history formed by repeatedly following a given loading path domain that contains all points from the stress or strain variations along one of its periods. Assume that two out-of-phase shear stresses τ_B and τ_A act parallel to the critical plane, where the crack will most likely initiate. Both τ_B and τ_A influence the growth of shear cracks along the critical plane. To calculate the maximum shear stress range $\Delta\tau_{max}$ at the critical plane, it is necessary to draw

* *Corresponding author.*
E-mail: meggi@puc-rio.br (M.A. Meggiolaro).
http://dx.doi.org/10.1016/j.jmrt.2015.01.004

Nomenclature

bc	Coffin–Manson's strain-life exponents
dp	length of an infinitesimal segment of the stress or strain path
E	Young's modulus
I_ε, I_γ, $I_{\varepsilon\gamma}$	moments of inertia of the strain path with respect to the mean component
I^O_ε, I^O_γ, $I^O_{\varepsilon\gamma}$	moments of inertia of the strain path with respect to the diagram origin
I_σ, I_τ, $I_{\sigma\tau}$	moments of inertia of the stress path with respect to the mean component
I^O_σ, I^O_τ, $I^O_{\sigma\tau}$	moments of inertia of the stress path with respect to the diagram origin
N	fatigue initiation life in number of cycles
p	perimeter of the stress or strain path
$\Delta\gamma_{max}$	maximum shear strain range
$\Delta\sigma_{Mises}$	equivalent von Mises stress range
$\Delta\tau_{max}$	maximum shear stress range
ε_x	normal strain from tension–torsion history
ε_{xm}	mean normal strain from tension–torsion history
γ_A, γ_B	shear strains on the crack initiation plane
γ_{xy}	shear strain from tension–torsion history
γ_{xym}	mean shear strain from tension–torsion history
σ_x	normal stress from tension–torsion history
σ_{xm}	mean normal stress from tension–torsion history
τ_A, τ_B	shear stresses on the crack initiation plane
τ_{xy}	shear stress from tension–torsion history
τ_{xym}	mean shear stress from tension–torsion history

the path of the shear stress history along a $\tau_B \times \tau_A$ diagram, as shown in Fig. 1 (left). Analogously, for a given shear strain history, a similar approach can be followed to find the maximum shear strain range $\Delta\gamma_{max}$ at the critical plane from the shear strain path along a $\gamma_B \times \gamma_A$ diagram, see Fig. 1 (left).

The search for an effective range using the deviatoric stress path started with the pioneering work of van Dang [10], who studied various methods to define and calculate it. Since then, several "enclosing surface methods" have been proposed [2–9,11], which try to find circles, ellipses, or rectangles that contain the entire load path (in the 2D case). In a nutshell, in the 2D case, the minimum ball (MB) method [11] searches for the circle with minimum radius that contains the stress or strain path; the minimum ellipse (ME) methods [2–6] search for a path-enclosing ellipse with semi-axes a and b with minimum area $\pi \cdot a \cdot b$ or minimum norm $(a^2 + b^2)^{1/2}$; and the maximum prismatic hull (MPH) methods [5,7–9] search among the smallest path-enclosing rectangles the one with maximum area or maximum diagonal (its a max–min search problem). The value of $\Delta\tau_{max}$ or $\Delta\gamma_{max}$ in Fig. 1 (left) would either be assumed as the value of the circle diameter, or twice the ellipse norm, or the length of the enclosing rectangle diagonal.

The enclosing surface methods can also be applied to tension–torsion load histories, if a $\sigma_x \times \tau_{xy}\sqrt{3}$ diagram is considered. The effective range in this case is the von Mises stress range $\Delta\sigma_{Mises}$. Similarly, for tension–torsion histories where plastic strains dominate, a strain diagram $\varepsilon_x \times \gamma_{xy}/\sqrt{3}$ can be used to predict an effective von Mises strain range $\Delta\varepsilon_{Mises}$. These ranges could be used in an invariant-based damage model such as Sines or Crossland [1], which do not involve the projection of the stress or strain path onto candidate planes.

Such enclosing surface methods can be extended to histories involving more than two stress or strain components. E.g., if the history path is plotted in a 3D diagram $s_i \times s_j \times s_k$ or $e_i \times e_j \times e_k$ representing respectively three deviatoric stress or strain components, then the enclosing surface methods will search for spheres, ellipsoids, or rectangular prisms, as shown in Fig. 1 (right) for the sphere from the MB method [11]. For load paths represented in higher dimension diagrams, required for a general 6D multiaxial history, the search is for hyperspheres, hyperellipsoids, and rectangular hyperprisms.

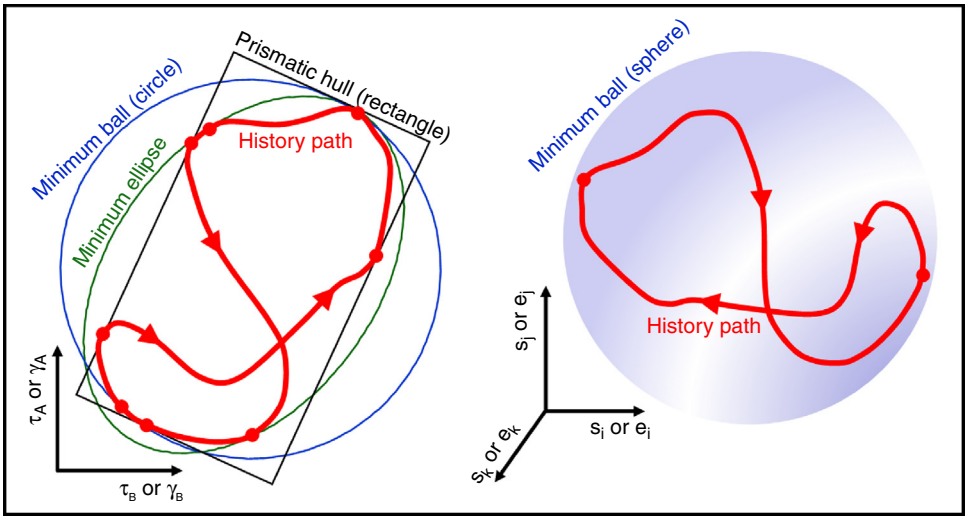

Fig. 1 – Left: periodic (or single) stress history path D in a $\tau_B \times \tau_A$ or $\gamma_B \times \gamma_A$ diagram, enclosed in surfaces such as circles (balls), ellipses, and rectangular prisms [12]; right: stress or strain path in a 3D sub-space of the E_{5s} or E_{5e} deviatoric spaces, circumscribed by a spherical convex enclosure.

In summary, the critical-plane approach requires the projection of the original history onto candidate planes, whose shear components are represented in 2D $\tau_B \times \tau_A$ or $\gamma_B \times \gamma_A$ diagrams to find the maximum shear range $\Delta\tau_{max}$ or $\Delta\gamma_{max}$ to be used, e.g., in Findley's or Fatemi–Socie's multiaxial damage models [1]. On the other hand, invariant-based approaches, such as the ones from the Sines and Crossland models, require the calculation of equivalent von Mises ranges $\Delta\sigma_{Mises}$ or $\Delta\varepsilon_{Mises}$ directly from the original history, without any plane projection, thus analyzing load paths represented in diagrams with higher dimension. In this work, only load paths represented in 2D will be considered, which would cover all critical-plane approaches (which only require an equivalent range calculation in a 2D $\tau_B \times \tau_A$ or $\gamma_B \times \gamma_A$ diagram), as well as invariant-based approaches for 2D tension–torsion histories.

Enclosing surface methods can be useful to estimate the equivalent stress (or strain) amplitude associated with NP loading paths, for both critical-plane and invariant-based approaches. However, such methods have three issues. First, among all enclosing surface methods, only the MB has a physical foundation. The search for the minimum ball enclosing a history path in the deviatoric space corresponds to the search of the elastic-shakedown state that the material grains in the neighbor of the point of interest could attain under periodic loading, considering an isotropic and/or kinematic hardening behavior. In other words, fatigue crack initiation is avoided if an elastic shakedown state can be reached. On the other hand, enclosing ellipsoids and prisms are not derived from physical considerations, they are empirical methods that try to interpolate the limit cases between a proportional loading history and a highly non-proportional one. Even so, these methods still have their practical value as engineering tools for relatively simple loading paths, as long as their effectiveness is experimentally verified.

The second issue with enclosing surface methods is that each portion of the considered path should not involve more than 1 cycle. Otherwise, if it is considered as a single cycle, the actual damage might be underestimated. Instead, a multiaxial rainflow algorithm should be applied to the entire stress or strain history, and then an enclosing surface method should be applied for the path of each rainflow-counted reversal.

Finally, the third issue involves information loss. Enclosing surface algorithms do not take into account the actual loading path, but only the convex enclosures associated with them. For instance, consider a square path ABCD in a 2D deviatoric space. The convex hull of such path, defined as the convex enclosure with minimum area that contains the entire path, is the square itself. An hourglass-shaped path ABDC or ADBC would have the same convex enclosure: the square ABCD. It is not difficult to prove that the enclosing circle, ellipse, or prismatic hull from any existing enclosing surface method would result in the same enclosure for these three considered paths, treating them as identical. In general, all paths that share the same convex hull share as well the same enclosing surface for a given method, even though they might lead to different equivalent amplitudes and fatigue lives. This third issue is addressed by the moment of inertia (MOI) method, originally proposed by the authors in [12], which calculates equivalent and mean components while taking into account the actual loading path, not only its convex enclosure. In this work, the formulation of the MOI method is adapted to predict the equivalent stress or strain ranges in NP tension–torsion histories, as presented next.

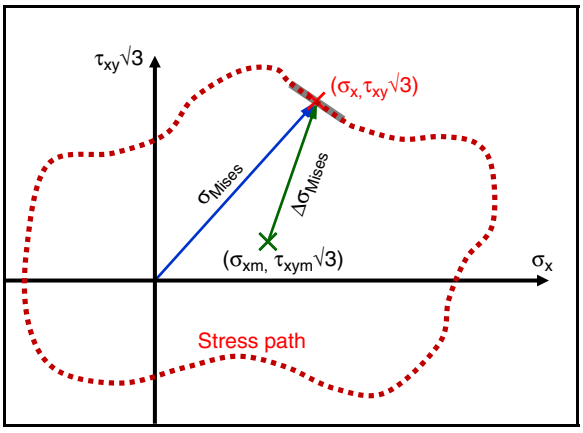

Fig. 2 – Tension–torsion path in the $\sigma_x \times \tau_{xy}\sqrt{3}$ space, along with its mean component (σ_{xm}, $\tau_{xym}\sqrt{3}$).

2. The moment of inertia (MOI) method

The moment of inertia (MOI) method aims to calculate alternate and mean components of complex NP load histories. The load history is first represented in a 2D deviatoric subspace, whose metric should be proportional to the maximum shear or to the von Mises equivalent stress or strain. Therefore, for critical-plane approaches, the shear-shear diagrams $\tau_B \times \tau_A$ or $\gamma_B \times \gamma_A$ are appropriate, since their metric (the distance between two stress or strain states) can be used in the calculation of the maximum shear range $\Delta\tau_{max}$ or $\Delta\gamma_{max}$. For tension–torsion histories using an invariant-based approach, the $\sigma_x \times \tau_{xy}\sqrt{3}$ stress diagram is a good choice since its metric is proportional to the von Mises equivalent stress $(\sigma_x^2 + 3\tau_{xy}^2)^{1/2}$. Note that the metric of the usually adopted $\varepsilon_x \times \gamma_{xy}/\sqrt{3}$ strain diagram is only proportional to the von Mises equivalent strain if plastic strains dominate, otherwise elastic Poisson effects would make its metric slightly different. Nevertheless, both $\sigma_x \times \tau_{xy}\sqrt{3}$ and $\varepsilon_x \times \gamma_{xy}/\sqrt{3}$ diagrams are usually adopted regardless of this small issue.

Once the load history is represented in the adopted stress or strain diagram, the MOI method assumes that the 2D load path can be regarded as a homogeneous wire with unit mass. For simplicity, the following derivations will assume a tension–torsion stress path using a $\sigma_x \times \tau_{xy}\sqrt{3}$ diagram, represented by a series of points $(\sigma_x, \tau_{xy}\sqrt{3})$ from the stress variations along it, see Fig. 2, or a $\varepsilon_x \times \gamma_{xy}/\sqrt{3}$ diagram, represented by a series of points $(\varepsilon_x, \gamma_{xy}/\sqrt{3})$ from the strain variations. Note that the formulation detailed below could be easily adapted to load paths in $\tau_B \times \tau_A$ or $\gamma_B \times \gamma_A$ diagrams, useful for the critical plane approach in the search for initiating mixed Modes II–III microcracks.

In the MOI method, the load path mean component is located at the center of mass of this hypothetical homogeneous wire with the shape of the history path. For the tension–torsion case shown in Fig. 2, such center of gravity

is located at the perimeter centroid (σ_{xm}, $\tau_{xym}\sqrt{3}$), calculated from integrals along the stress path

$$\sigma_{xm} = \frac{1}{p}\cdot\int \sigma_x \cdot dp, \quad \tau_{xym}\sqrt{3} = \frac{1}{p}\cdot\int \tau_{xy}\sqrt{3}\cdot dp,$$
$$p = \int dp, \quad dp \equiv \sqrt{d\sigma_x^2 + 3\cdot d\tau_{xy}^2} \tag{1}$$

where p is the path perimeter and dp is the length of an infinitesimal segment of the path. Analogously for strain histories, the perimeter centroid (ε_{xm}, $\gamma_{xym}/\sqrt{3}$) is calculated from

$$\varepsilon_{xm} = \frac{1}{p}\cdot\int \varepsilon_x \cdot dp, \quad \frac{\gamma_{xym}}{\sqrt{3}} = \frac{1}{p}\cdot\int \frac{\gamma_{xy}}{\sqrt{3}}\cdot dp, \quad p = \int dp,$$
$$dp \equiv \sqrt{d\varepsilon_x^2 + \frac{d\gamma_{xy}^2}{3}} \tag{2}$$

The mass moments of inertia (MOI) of this hypothetical wire are then used by the MOI, giving the method its name, calculated with respect to the origin O of the stress diagram, assuming the wire has unit mass, resulting in

$$I_\sigma^O = \frac{1}{p}\times\int (\tau_{xy}\sqrt{3})^2\cdot dp, \quad I_\tau^O = \frac{1}{p}\times\int (\sigma_x)^2\cdot dp,$$
$$I_{\sigma\tau}^O = -\frac{1}{p}\cdot\int (\sigma_x)(\tau_{xy}\sqrt{3})\cdot dp \tag{3}$$

The parallel axis theorem for a unit mass is then used to calculate the respective MOI with respect to the center (σ_{xm}, $\tau_{xym}\sqrt{3}$) of the path, giving:

$$I_\sigma = I_\sigma^O - (\tau_{xym}\sqrt{3})^2, \quad I_\tau = I_\tau^O - (\sigma_{xm})^2,$$
$$I_{\sigma\tau} = I_{\sigma\tau}^O + (\sigma_{xm})(\tau_{xym}\sqrt{3}) \tag{4}$$

Analogously for strain-controlled histories, the moments of the strain path with respect to the diagram origin become

$$I_\varepsilon^O = \frac{1}{p}\cdot\int (\gamma_{xy}/\sqrt{3})^2\cdot dp, \quad I_\gamma^O = \frac{1}{p}\cdot\int (\varepsilon_x)^2\cdot dp,$$
$$I_{\varepsilon\gamma}^O = -\frac{1}{p}\cdot\int (\varepsilon_x)\left(\frac{\gamma_{xy}}{\sqrt{3}}\right)\cdot dp \tag{5}$$

while the respective values with respect to the center (ε_{xm}, $\gamma_{xym}/\sqrt{3}$) of the path are:

$$I_\varepsilon = I_\varepsilon^O - \left(\frac{\gamma_{xym}}{\sqrt{3}}\right)^2, \quad I_\gamma = I_\gamma^O - (\varepsilon_{xm})^2, \quad I_{\varepsilon\gamma} = I_{\varepsilon\gamma}^O + (\varepsilon_{xm})\left(\frac{\gamma_{xym}}{\sqrt{3}}\right) \tag{6}$$

In the MOI method, the von Mises stress range $\Delta\sigma_{Mises}$ (or the strain range $\Delta\varepsilon_{Mises}$ for strain paths) is assumed to depend on the mass moment of inertia I_z with respect to the path centroid, perpendicular to the stress diagram, which is equal to the sum of the moments of inertia in σ and in τ, respectively I_σ and I_τ (or to the sum of I_ε and I_γ, for strain paths). Thus, history paths further away from their perimeter centroid contribute more to the effective range and amplitude. The MOI method states that the equivalent von Mises ranges of the stress or strain paths are then

$$\Delta\sigma_{Mises} = \sqrt{12\cdot(l_\sigma + l\tau)} \text{ or } \Delta\varepsilon_{Mises}(1-\bar{\nu}) = \sqrt{12\cdot(l_\varepsilon + l_\gamma)} \tag{7}$$

where $\bar{\nu}$ is an effective Poisson ratio. These equations are coherent with the fact that a proportional loading path with length L will result in the expected range $\Delta\sigma_{Mises}$ or $\Delta\varepsilon_{Mises}(1-\bar{\nu})$ equal to L, since the MOI of a straight rod element with respect to its centroid is $m{\cdot}L^2/12$.

The MOI method can also be applied to polygonal load history paths, which is useful for discrete computer implementations. If each side i of the polygon has length Δp_i, centered at (σ_{xmi}, $\tau_{xymi}\sqrt{3}$), and making an angle ψ_i with respect to the horizontal, then

$$p = \sum_i \Delta p_i, \quad \sigma_{x_m} = \frac{1}{p}\cdot\sum_i \sigma_{x_{m_i}}\cdot\Delta p_i,$$
$$\tau_{xy_m}\sqrt{3} = \frac{1}{p}\cdot\sum_i \tau_{xy_{m_i}}\sqrt{3}\cdot\Delta p_i$$
$$I_\sigma^O = \frac{1}{p}\cdot\sum_i\left(\frac{\Delta p_i^2}{12}\sin^2\psi_i + (\tau_{xy_{m_i}}\sqrt{3})^2\right)\cdot\Delta p_i,$$
$$I_\tau^O = \frac{1}{p}\cdot\sum_i\left(\frac{\Delta p_i^2}{12}\cos^2\psi_i + (\sigma_{x_{m_i}})^2\right)\cdot\Delta p_i$$
$$I_\sigma^O = -\frac{1}{p}\cdot\sum_i\left(\frac{\Delta p_i^2}{12}\sin\psi_i\cos\psi_i + (\sigma_{x_{m_i}})(\tau_{xy_{m_i}}\sqrt{3})\right)\cdot\Delta p_i \tag{8}$$

Analogous expressions can be derived for strain histories.

The equivalent ranges are then calculated from Eqs. (3) and (4). In the next section, the MOI and enclosing surface methods are compared against experimental data gathered from the literature.

3. Experimental evaluation of the MOI and enclosing surface fatigue life predictions

To evaluate the MOI method and enclosing surface estimates of effective ranges, 13 periodic histories are studied, represented by the block loadings shown in Fig. 3 for Cases 0–12. These strain-controlled tension–torsion histories were performed in [13] using 304 stainless steel specimens. The multiaxial fatigue lives are calculated using the Smith–Watson–Topper (SWT) model [14] with the von Mises strain amplitudes calculated from the MOI method. The material properties used in these calculations are:

$$\varepsilon = \frac{\sigma}{E} + \left(\frac{\sigma}{1754}\right)^{1/0.276}$$
$$\left(\sigma_{max}\frac{\Delta\varepsilon}{2}\right)_{max} = \frac{757^2}{E}(2N)^{2b} + 30.5\cdot(2N)^{b+c} \tag{9}$$
$$E = 197,000\,\text{MPa}, \quad b = -0.0886, \quad c = -0.303$$

Table 1 – Fatigue life N (in cycles) experimentally measured and predicted using the Smith–Watson–Topper damage model and the moment of inertia (MOI), minimum ball (MB), and maximum prismatic hull (MPH) methods, along with percent differences, marked in gray for errors of 30% or more. Note that Cases 1–4 consider 2 cycles per block (e.g. the measured life for Case 1 was 1400 loading blocks, and thus shown as 2800 cycles).

Path	Measured	MOI		MB		MPH	
Case 0	7100	7085	0%	7085	0%	7085	0%
Case 1	2800	3379	21%	3379	21%	1150	−59%
Case 2	4200	4462	6%	4462	6%	1504	−64%
Case 3	820	640	−22%	640	−22%	229	−72%
Case 4	900	858	−5%	858	−5%	304	−66%
Case 5	3200	3557	11%	3557	11%	3557	11%
Case 6	2600	2332	−10%	2393	−8%	2177	−16%
Case 7	1700	1590	−6%	1751	3%	1453	−15%
Case 8	470	604	29%	856	82%	572	22%
Case 9	660	604	−8%	856	30%	572	−13%
Case 10	320	329	3%	949	196%	329	3%
Case 11	1200	1073	−11%	2241	87%	1073	−11%
Case 12	710	689	−3%	2023	185%	689	−3%

Table 1 shows the experimental fatigue lives and the associated predictions using the MOI, minimum ball (MB), and maximum prismatic hull (MPH) methods, for each one of the 13 loading histories. Note that the MOI method considers two cycles per load block for Cases 1–4; this number of cycles can be deterministically obtained using the Modified Wang–Brown rainflow algorithm described in [15].

Cases 0–5 are expected to be proportional, because star or cross-shaped histories (from Cases 1 to 4) are the combination of two independent perpendicular proportional paths. Both MOI and MB methods are able to capture that, however the MPH combines these two perpendicular paths into a single non-proportional path, even though they will most likely induce perpendicular cracks that do not interact. Therefore, the MPH generates very conservative predictions in these cases (marked in gray in Table 1), because it is not able to distinguish e.g. between a cross-shaped and a circular history. The MOI method life predictions are also relatively accurate for the remaining load cases. Note however that the MB method assumes that all studied load cases are proportional, resulting in non-conservative predictions for the significantly non-proportional Cases 8–12 (also marked in gray in Table 1).

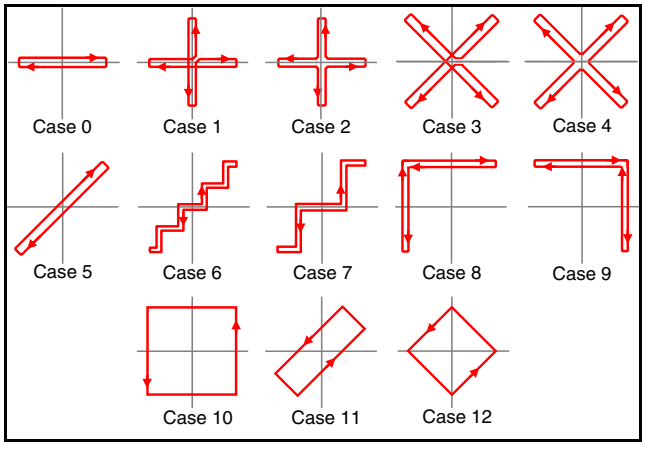

Fig. 3 – History paths used in the experimental validation of the equivalent range predictions.

The MOI-predicted initiation lives end up within 30% from the experimental results for all 13 histories. The MPH method wrongfully assumes that cross or star-shaped histories are 90° out-of-phase, instead of being proportional; therefore, the MPH is more appropriate for convex load paths to avoid overly conservative predictions. The MB method, on the other hand, results in non-conservative predictions for non-proportional histories such as Cases 8–12, since it wrongfully assumes that these paths are proportional.

The main limitation of the presented version of the MOI method is its application only for 2D stress or strain paths. In the critical-plane approach, this is not a problem since the only required equivalent range is the one associated with the two shear stress or strain components on the candidate plane, which is a 2D problem even for a 6D non-proportional history. On the other hand, in the invariant-based approach such as in Crossland's model, the presented 2D formulation would be able to deal with tension–torsion histories and perhaps extended to biaxial normal histories, but a more general stress state would require a higher-dimension version of the MOI method.

4. Conclusions

A method to calculate equivalent ranges in multiaxial histories, called the moment of inertia (MOI) method, was presented using a tension–torsion formulation. Since the MOI is not based on load path enclosures, it better deals with path-shape dependence issues, including non-convex paths. Experimental results for 13 different multiaxial histories collected from the literature proved the effectiveness of the MOI method to predict the associated fatigue lives, when compared to the existing enclosing surface methods.

Conflicts of interest

The authors declare no conflicts of interest.

REFERENCES

[1] Socie DF, Marquis GB. Multiaxial fatigue. Warrendale, PA: Society of Automotive Engineers, Inc.; 2000.

[2] Freitas M, Li B, Santos JLT. A numerical approach for high-cycle fatigue life prediction with multiaxial loading. In: Multiaxial fatigue and deformation: testing and prediction, ASTM STP 1387. ASTM; 2000.

[3] Li B, Santos JLT, Freitas M. A unified numerical approach for multiaxial fatigue limit evaluation. Mech Struct Mach 2000;28:85–103.

[4] Li B, Santos JLT, Freitas M. A computerized procedure for long-life fatigue assessment under multiaxial loading. Fatigue Fract Eng Mater Struct 2001;24:165–77.

[5] Gonçalves CA, Araújo JA, Mamiya EN. Multiaxial fatigue: a stress based criterion for hard metals. Int J Fatigue 2005;27:177–87.

[6] Zouain N, Mamiya EN, Comes F. Using enclosing ellipsoids in multiaxial fatigue strength criteria. Eur J Mech A: Solids 2006;25:51–71.

[7] Mamiya EN, Araújo JA, Castro FC. Prismatic hull: a new measure of shear stress amplitude in multiaxial high cycle fatigue. Int J Fatigue 2009;31:1144–53.

[8] Castro FC, Araújo JA, Mamiya EN, Zouain N. Remarks on multiaxial fatigue limit criteria based on prismatic hulls and ellipsoids. Int J Fatigue 2009;31:1875–81.

[9] Araújo JA, Dantas AP, Castro FC, Mamiya EN, Ferreira JLA. On the characterization of the critical plane with a simple and fast alternative measure of the shear stress amplitude in multiaxial fatigue. Int J Fatigue 2011;33:1092–100.

[10] van Dang K. Macro-micro approach in high-cycle multiaxial fatigue. ASTM STP 1191. ASTM; 1993.

[11] van Dang K, Papadopoulos IV. High-cycle metal fatigue. Springer 1999.

[12] Meggiolaro MA, Castro JTP. An improved multiaxial rainflow algorithm for non-proportional stress or strain histories: Part I. Enclosing surface methods. Int J Fatigue 2012;42:217–26.

[13] Kida S, Itoh T, Sakane M, Ohnami M, Socie DF. Dislocation structure and non-proportional hardening of type 304 stainless steel. Fatigue Fract Eng Mater Struct 1997;20:1375–86.

[14] Smith RN, Watson P, Topper TH. A stress–strain parameter for the fatigue of metals. J Mater 1970;5:767–78.

[15] Meggiolaro MA, Castro JTP. An improved multiaxial rainflow algorithm for non-proportional stress or strain histories: Part II. The modified Wang-Brown method. Int J Fatigue 2012;42:194–206.